Shading the TRF2 Recruiting Function: A New Horizon in Drug Development

Salvatore Di Maro,[#,○] Pasquale Zizza,[‡,○] Erica Salvati,[‡] Viviana De Luca,[§] Clemente Capasso,[§] Iolanda Fotticchia,[†] Bruno Pagano,[†] Luciana Marinelli,[†] Eric Gilson,[∥,⊥] Ettore Novellino,[†] Sandro Cosconati,*[#] and Annamaria Biroccio[‡]

[#]DiSTABiF, Second University of Naples, Caserta, Italy

[‡]Experimental Chemotherapy Laboratory, Regina Elena National Cancer Institute, Rome, Italy

[§]Istituto di Biochimica delle Proteine-CNR, Napoli, Italy

[†]Department of Pharmacy, University of Naples "Federico II", Napoli, Italy

[∥]Institute for Research on Cancer and Aging, Nice (IRCAN), Nice University, CNRS UMR7284/INSERM U1081, Faculty of Medicine, Nice, France

[⊥]Department of Medical Genetics, Archet 2 Hospital, CHU of Nice, Nice, France

S *Supporting Information*

ABSTRACT: The shelterin protein TRF2 has come to the limelight for its role in telomere maintenance and tumorigenesis. Herein, the application of rational design and synthesis allowed identifying the first TRF2$_{TRFH}$ binder able to elicit a marked DNA damage response in cancer cells. This work paves the way for the unprecedented employment of a chemical tool to finely tune specific mechanisms underlying telomere maintenance.

Telomeres are key features of chromosome termini that preserve genome integrity.[1] In many organisms, their protective function depends upon at least two pathways. The first relies on telomerase, which can compensate for replicative erosion,[2] and the second relies on a particular nucleoprotein complex named "shelterin", protecting chromosome ends from aberrant signaling and repair.[3] In mammalian cells, protection of chromosome ends requires the shelterin protein telomeric repeat-binding factor 2 (TRF2). Indeed, TRF2 helps the folding of telomeric DNA into a t-loop, which might contribute to telomere protection by masking the 3′-end overhang from being recognized as damaged DNA, preventing activation of a DNA damage response (DDR) at telomeres and inappropriate repair.[4,5] Moreover, when telomeres become critically short, insufficient recruitment of TRF2 leads to telomere deprotection and initiation of a DDR pathway at chromosome ends.[6] Full suppression of TRF2 activates the same response as critically short telomeres, such as recruitment of DDR factors, activation of a cell cycle checkpoint, and repair activities resulting in chromosome fusions.[7] On the other hand, partial localization of TRF2 at telomeres, while not leading to chromosome end-to-end fusions, forces cells to G1 arrest or genome instability depending on the cell p53 competence.[8] More recently, a two-step mechanism for TRF2-mediated end protection has been identified: first the dimerization domain of TRF2 (TRF2$_{TRFH}$) is required to prevent ATM kinase activation; next, TRF2,

through a portion of the hinge domain (iDDR), can suppress the propagation of DNA damage signaling.[9] The anti-ATM effect of TRF2$_{TRFH}$ could stem from its ability to modify the topological conformation of telomeric DNA and/or from its interaction with different proteins sharing a specific amminoacidic motif ([Y/F/H]xLxP; x: any amino acid).[5,10] The capacity of TRF2$_{TRFH}$ to bind several different molecular partners sharing a common recognition motif indicates that an array of TRF2 molecules serves as a protein hub for different signaling.

Interestingly, increased expression of TRF2, observed in human malignancies,[11,12] contributes to carcinogenesis in mice[13] and is regulated by the Wnt/β-catenin pathway.[14] Moreover, overexpression of TRF2 is required for tumorigenicity, not only by a delay of replicative senescence but also by a noncell autonomous mechanism preventing innate immune surveillance and relying on extra-telomeric roles of TRF2 in gene expression regulation.[15] Likely, in tumor cells, overexpression of TRF2 can trigger aberrant signaling pathways by engaging interactions with different molecular partners, contributing to cancer progression ad maintenance. These recent advances in the comprehension of the multiple roles exerted by TRF2 indicate this protein as an interesting target for the development of interacting chemicals that serve as tools for both basic and translational cancer research. In particular, genetic disruption of the TRF2$_{TRFH}$ domain interactions impairs telomere maintenance and elicits a DDR signaling, thereby suggesting this domain as a pertinent drug target.[9] Herein, a structure-based rational design has been applied in tandem with a targeted peptide synthesis to discover the first chemotypes that directly bind TRF2$_{TRFH}$, thereby switching off its recruiting functions. The design campaign started with the analysis of the available X-ray structures of this domain in complex with the C-terminus of Apollo (Apo$_{TBM}$, Apollo 496−532, PDB 3BUA) and with a short fragment of SLX4 (SLX4$_{TBM}$, SLX4 1014−1028, PDB 4M7C), two non-shelterin molecular partners of TRF2$_{TRFH}$ involved in telomere

protection.[16−18] The two peptides bind the TRF2$_{TRFH}$ by adopting a similar conformation and interaction pattern (Figure 1a), in which a random coil followed by a short α-helix turn fits in
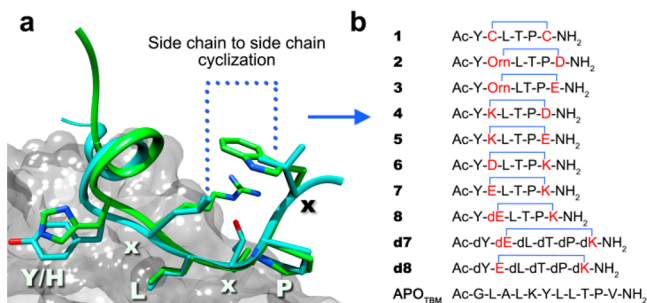

Figure 1. (a) Design of cyclic peptides to recapitulate the experimental Apo$_{TBM}$ and SLX4$_{TBM}$ binding conformation in complex with TRF2$_{TRFH}$. The protein is depicted as a gray surface, while Apo$_{TBM}$ and SLX4$_{TBM}$ are depicted as cyan and green sticks and ribbons, respectively. (b) Sequences of the designed peptides.

the narrow gorge of TRF2$_{TRFH}$ where the [Y/F/H]xLxP motif engages hydrophobic (L and P) and polar contacts (Y/H).

Thus, the most straightforward approach to design a TRF2$_{TRFH}$ binder was to start with a peptide structure featuring the Y/HxLxP binding motif devoid of the flanking residues which were not shown to be critical for protein−protein interactions. Moreover, since we were interested in a chemotype endowed with better binding affinity for the target as well as cell-penetrating properties, we decided to induce conformational constraints by designing cyclic peptides. The best cyclization strategy was to attain a side chain-to-side chain cyclization by mutating L505 and V509 (Apo$_{TBM}$ numbering) in specific residues allowing for a variety of chemical bonds. This choice was dictated by several considerations: (i) the aforementioned residues are spatially closed to each other in the experimental Apo$_{TBM}$ bound conformation, (ii) they do not engage tight interactions with TRF2$_{TRFH}$, and (iii) the resulting pentapeptide would have a limited conformational flexibility. As reported in Figure 1b this cyclization strategy leaves the Y residue to be exocyclic.

Therefore, a small library of conformationally restricted peptides was designed by inserting amino acids, such as C, K, Orn, D, E, bearing side chains that could be easily connected through disulfide (**1**) and lactam bridges (**2**−**7**) (Figure 1b). All peptides were synthesized by a Nα-Fmoc/*tert*-butyl strategy of solid-phase peptide chemistry and then tested in an *in vitro* assay for the semiquantitative measure of their binding affinity to TRF2$_{TRFH}$. Specifically, a GST-tagged TRFH domain, able to bind an HA-tagged peptide featuring the binding motif of Apo$_{TBM}$ (Figure S1), was used in a competitive pull-down assay in which we compared the binding of the HA-tagged peptide to GST-TRFH, in the absence (negative control) or presence of the equimolar concentrations of the selected peptides. Results, showing the amount of TRF2$_{TRFH}$-bound HA-peptide, clearly indicate that **7** was the most potent binder, being able to reduce by about 70% the binding of the HA-tagged peptide (Figure 2a). Molecular modeling studies were then attained to provide at atomic level a clearer picture of the interaction established by peptide **7** and TRF2$_{TRFH}$. To this end, replica-exchange molecular dynamics (REMD) simulations were first used to computationally presample the peptide low free-energy conformational basins of **7** in solution. Results of our 4 μs REMD
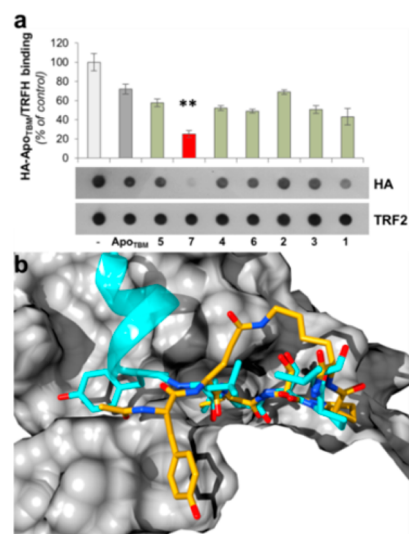
Figure 2. (a) Competitive binding assay. Matrix bound GST-TRF2TRFH was incubated with equimolar concentrations of HA-Apo$_{TBM}$ and **1**−**7** peptides. Apo$_{TBM}$ alone was used as the control. Matrix bound proteins were eluted and analyzed by dot blot against HA. Histograms report densitometries of anti-HA signals (normalized on relative TRF2 signals) expressed as the percentage of control. A signal decrease revealed the interference of **1**−**7** with HA-Apo$_{TBM}$ binding to TRF2 protein. The mean of three independent experiments with comparable results is shown. Error bars indicate SD ($**$ = $p < 0.01$). (b) Predicted **7**/TRF2TRFH complex. The ligand is represented as yellow sticks while protein is represented as a gray surface; the Apo$_{TBM}$ cocrystal structure, depicted as cyan ribbons and sticks, is also reported as reference.

simulations were analyzed considering the peptide conformations adopted at 300 K that were subsequently clustered employing the average linkage method and a cluster member cutoff of 0.5 Å rmsd calculated on the Cα carbons of the peptide residues within the cycle. The 22 calculated conformations, representative of each conformational cluster, were then considered in subsequent docking studies attained with the AutoDock 4.2 software (AD4) and employing the TRF2$_{TRFH}$ structure having PDB code 3BUA (see methods for full explanation of this methodology). In the lowest energy conformation calculated by AD4 the ligand is able to adapt in the protein binding site strongly resembling the binding mode of the cocrystal peptides (see Figures 2b and S2) with the exception of Y^1 that is lodged in a cleft adjacent to that hosting the Y and H residues of the cocrystal Apo$_{TBM}$ and SLX4$_{TBM}$ peptides, respectively. Analysis of these differences made clear that the different binding position of Y^1 in **7** could be ascribed to the chirality of the cα carbon of E^2 and, in principle, replacing it with the D-amino acid (dE^2) would have led to a new peptide that could better recapitulate the experimental peptide/protein interactions.

To test the viability of this hypothesis, the above-described computational protocol was applied to peptide **8** featuring dE^2 and suggested that this latter peptide would be able to recapitulate the whole interaction pattern recorded for the cocrystal peptides in the X-ray studies (Figures 3a and S3). While the results of these computational studies seem to indicate that **8** is more prone to recapitulate the cocrystal linear peptides, this does not necessarily mean that this would result in higher binding affinities. Thus, **8** was synthesized and assayed for its affinity to TRF2$_{TRFH}$. The *in vitro* binding experiments revealed that **7** and

16709

dx.doi.org/10.1021/ja5080773 | *J. Am. Chem. Soc.* 2014, 136, 16708−16711
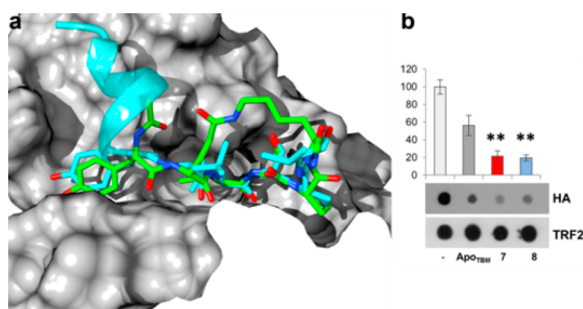
Figure 3. (a) Predicted **8**/TRF2$_{TRFH}$ complex and sequence of the peptide. The ligand is represented as green sticks while protein is represented as a gray surface; the Apo$_{TBM}$ cocrystal structure, depicted as cyan ribbons and sticks, is also reported as reference. (b) Competitive binding assay of HA-Apo$_{TBM}$ with **7** and **8** analyzed as described above. The mean of three independent experiments with comparable results is shown. Error bars indicate SD (* = $p < 0.01$). GST-TRF2$_{TRFH}$ was incubated with equimolar concentrations of HA-Apo$_{TBM}$ and **7** and **8** peptides.

8 shared a comparable effect in counteracting the interaction of Apo$_{TBM}$ with the TRF2$_{TRFH}$ (Figure 3b).

To investigate, from a thermodynamic point of view, similarities and/or differences between the interaction of TRF2$_{TRFH}$ with the binding partner Apo$_{TBM}$ and with peptides **7** and **8**, we performed isothermal titration calorimetric (ITC) experiments. ITC measurements showed that **7** and **8** interact with TRF2$_{TRFH}$ in vitro, with a 1:1 binding stoichiometry (Figure 4). The data show that Apo$_{TBM}$ and **7** have comparable affinity
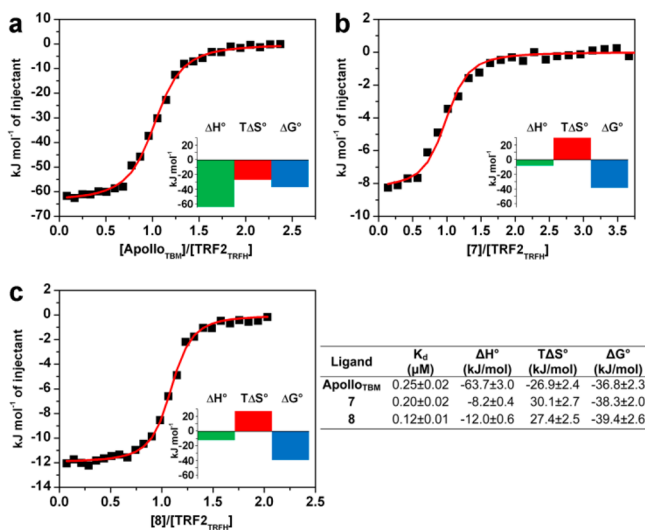

Figure 4. ITC binding isotherms and thermodynamic signatures (insets) for titration of TRF2$_{TRFH}$ with Apo$_{TBM}$ (a), **7** (b), and **8** (c) peptides obtained at 25 °C. The squares represent the experimental data obtained by integrating the raw ITC data and subtracting the heat of peptide dilution into the buffer. The red lines represent the best fit obtained by fitting the experimental binding isotherm to an equivalent and independent-sites model.

for TRF2$_{TRFH}$ (K_d = 0.25 and 0.20 μM, respectively). On the other hand, the structural modifications introduced in **8** resulted in a higher affinity (K_d = 0.12 μM), probably as a consequence of the better recapitulation of the Apo$_{TBM}$/TRF2$_{TRFH}$ interactions. Noteworthy, the thermodynamic signatures for the binding of the cyclic peptides are very different if compared to the Apo$_{TBM}$ ones (Figure 4). Indeed, the less favorable enthalpy change

values measured for the interactions of **7** and **8** with TRF2$_{TRFH}$ (−8.2 and −12.0 kJ mol^{-1}, respectively) with respect to that recorded for Apo$_{TBM}$ (−63.7 kJ mol^{-1}) are explained by the absence, in the cyclic peptides, of the accessory interacting residues flanking the YxLxP binding motif of Apo$_{TBM}$. On the other hand, these less favorable enthalpy changes are fully compensated by a favorable entropic contribution to the binding (30.1 and 27.4 kJ mol^{-1} for **7** and **8**, respectively), which is unfavorable for Apo$_{TBM}$ (−26.9 kJ mol^{-1}) due to its intrinsic conformational freedom. These data substantiate the correctness of our initial hypothesis to design short and conformationally constrained peptides to achieve high binding affinity for TRF2$_{TRFH}$. Finally, **7** and **8** have been tested for their ability to trigger a DNA damage response in Hela cells as well as their stereoisomers **d7** and **d8** (Figure 1b) that were used as control peptides. Our results demonstrated that, consistently with already reported data,[10] both **7** and **8** did not modify the telomeric localization of TRF2 (Figure S4a). Also, the two peptides significantly increased the percentage of cells with phosphorylated H2AX (γH2AX) up to more than 50% when compared to control peptides (Figures S4b, 5a and b, S5a). In addition, γH2AX was activated in response to dysfunctional telomeres. Indeed, almost all the γH2AX positive cells exhibited more than 4 TRF1/γH2AX colocalizations (Figure 5a and b) with a mean of ~8 TIFs (Telomere-dysfunction Induced Foci) per nucleus, and interestingly, if compared to **7**, **8** showed a higher percentage of TRF1/γH2AX colocalizations (Figure 5b). Of note, only a small fraction of cells exhibited 53BP1 activation (Figures 5b and S5a), anaphase bridges indicative of end-to-end fusions (Figure S5b), and eventually died (Figure S5c).

Moreover, meta-TIFs assay, performed to accurately estimate the number of TIFs in an entire nucleus and to avoid the inclusion of TIFs postulated to transiently occur during the S/G2 phases, showed a huge activation of telomeric and nontelomeric γH2AX spots in discrete genomic loci (Figure 5c and d). The presence of nontelomeric γH2AX spots is consistent with the ability of TRF2 to bind and protect interstitial telomeric DNA sequences against DDR activation.[19] The degree of telomere deprotection accompanied by the almost complete lack of 53BP1 recruitment suggests that disruption of the TRF2$_{TRFH}$ inter-actions can induce a partially deprotected state in which the chromosome ends activate ATM/γH2AX but still protects against 53BP1 recruitment and/or spreading. The lack of a full DDR can be due to the presence of a DDR inhibitor domain outside the TRF2$_{TRFH}$ repressing the 53BP1 activation.[9] Genetic disruption of the TRF2$_{TRFH}$ domain interactions by the expression of a TRF2$_{TRFH}$ mutant has been recently reported to elicit the first step of the DNA damage response (γH2AX activation, without recruitment of 53BP1).[9] Therefore, the ability of the chemical compounds described here to reproduce the same cellular phenotype obtained with the mutational analysis of the TRF2$_{TRFH}$ indicates that this domain can be actually targeted and strongly supports the specificity of our compounds.

In conclusion, our results demonstrate that the proposed chemical modifications introduced in the ApoTBM binding motif significantly increase the affinity and the specificity of the peptide for TRF2$_{TRFH}$, thereby identifying the first cell-permeable TRF2 binding chemotype as a tool for both basic and translational research.

16710

dx.doi.org/10.1021/ja5080773 | *J. Am. Chem. Soc.* 2014, 136, 16708−16711
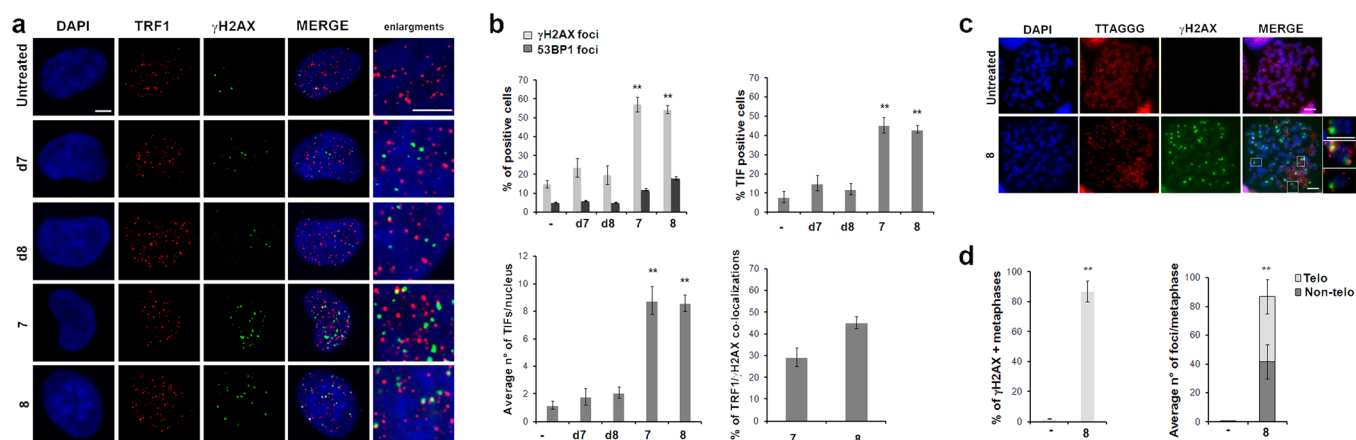
Figure 5. (a) Represenative images (100× magnification) of IF experiments performed in Hela cells treated for 24 h with 1 μM of the indicated compounds, stained with anti-TRF1 and -γH2AX antibodies, and finally counterstained with DAPI. (b) Quantitative analysis of the above samples in terms of percentage of cells positive for DDR markers and TIFs, average number of TIFs per nucleus and percentage of TIFs on the total number of damage spots. (c) Represenative metaphases (100× magnification) of cells treated as above and stained with γH2AX and hybridized with a red fluorescent telo-probe. (d) Quantitative analysis of the samples in c scored as percentage of γH2AX positive metaphases and average number of γH2AX labeled chromosomes in telomeric and nontelomeric regions. The mean of three independent experiments with comparable results is shown. Error bars indicate SD (* = $p < 0.1$ ** = $p < 0.01$). Scale bar = 5 μm.

ASSOCIATED CONTENT

S **Supporting Information**

Additional figures and tables, computational and experimental methods. This material is available free of charge via the Internet at http://pubs.acs.org.

AUTHOR INFORMATION

Corresponding Author

sandro.cosconati@unina2.it

Author Contributions

○S.D.M. and P.Z. contributed equally to this work.

Notes

The authors declare no competing financial interest.

ACKNOWLEDGMENTS

REFERENCES

(1) Blackburn, H.; Greider, W.; Szostak, W. *Nat. Med.* **2006**, *12*, 1133.

(2) Cech, T. R. *Cell* **2004**, *116*, 273−279.

(3) Palm, W.; de Lange, T. *Annu. Rev. Genet.* **2008**, *42*, 301.

(4) Griffith, J. D.; Comeau, L.; Rosenfield, S.; Stansel, R. M.; Bianchi, A.; Moss, H.; de Lange, T. *Cell* **1999**, *97*, 503.

(5) Amiard, S.; Doudeau, M.; Pinte, S.; Poulet, A.; Lenain, C.; Faivre-Moskalenko, C.; Angelov, D.; Hug, N.; Vindigni, A.; Bouvet, P.; Paoletti, J.; Gilson, E.; Giraud-Panis, M. J. *Nat. Struct. Mol. Biol.* **2007**, *14*, 147.

(6) d'Adda di Fagagna, F.; Reaper, P. M.; Clay-Farrace, L.; Fiegler, H.; Carr, P.; Von Zglinicki, T.; Saretzki, G.; Carter, N. P.; Jackson, S. P. *Nature* **2003**, *426*, 194.

(7) Karlseder, J.; Broccoli, D.; Dai, Y.; Hardy, S.; de Lange, T. *Science* **1999**, *283*, 1321.

(8) Cesare, A. J.; Hayashi, M. T.; Crabbe, L.; Kalseder, J. *Moll. Cell.* **2013**, *51*, 141.

(9) Okamoto, K.; Bartocci, C.; Ouzounov, I.; Diedrich, J. K.; Yates, J. R., III; Denchi, E. L. *Nature* **2013**, *494*, 502.

(10) Kim, H.; Lee, O. H.; Xin, H.; Chen, L. Y.; Qin, J.; Chae, H. K.; Lin, S. Y.; Safari, A.; Liu, D.; Songyang, Z. *Nat. Struct. Mol. Biol.* **2009**, *16*, 372.

(11) Nakanishi, K.; Kawai, T.; Kumaki, F.; Hiroi, S.; Mukai, M.; Ikeda, E.; Koering, C. E.; Gilson, E. *Clin. Cancer. Res.* **2003**, *9*, 1105.

(12) Diehl, M. C.; Idowu, M. O.; Kimmelshue, K. N.; York, T. P.; Jackson-Cook, C. K.; Turner, K. C.; Holt, S. E.; Elmore, L. W. *Breast Cancer Res. Treat.* **2011**, *127*, 623.

(13) Blanco, R.; Munoz, P.; Flores, J. M.; Klatt, P.; Blasco, M. A. *Genes Dev.* **2007**, *21*, 206.

(14) Diala, I.; Wagner, N.; Magdinier, F.; Shkreli, M.; Sirakov, M.; Bauwens, S.; Schluth-Bolard, C.; Simonet, T.; Renault, V. M.; Ye, J.; Djerbi, A.; Pineau, P.; Choi, J.; Artandi, S.; Dejean, A.; Plateroti, M.; Gilson, E. *EMBO Rep.* **2013**, *14*, 356.

(15) Ye, J.; Renault, V. M.; Jamet, K.; Gilson, E. *Nat. Rev. Genet.* **2014**, *15*, 491.

(16) Lenain, C.; Bauwens, S.; Amiard, S.; Brunori, M.; Giraud-Panis, M.-J.; Gilson, E. *Curr. Biol.* **2006**, *16*, 1303.

(17) van Overbeek, M.; de Lange, T. *Curr. Biol.* **2006**, *16*, 1295.

(18) Wan, B.; Yin, J.; Horvath, K.; Sarkar, J.; Chen, Y.; Wu, J.; Wan, K.; Lu, J.; Gu, P.; Yu, E. Y.; Lue, N. F.; Chang, S.; Liu, Y.; Lei, M. *Cell Rep* **2013**, *4*, 861.

(19) Ye, J.; Lenain, C.; Bauwens, S.; Rizzo, A.; Saint-Léger, A.; Poulet, A.; Benarroch, D.; Magdinier, F.; Morere, J.; Amiard, S.; Verhoeyen, E.; Britton, S.; Calsou, P.; Salles, B.; Bizard, A.; Nadal, M.; Salvati, E.; Sabatier, L.; Wu, Y.; Biroccio, A.; Londoño-Vallejo, A.; Giraud-Panis, M. J.; Gilson, E. *Cell* **2010**, *142*, 230.

16711

dx.doi.org/10.1021/ja5080773 | *J. Am. Chem. Soc.* 2014, 136, 16708−16711